NOTICE CONCERNING COPYRIGHT RESTRICTIONS

5956

CODA WAVE ATTENUATION AND ORIGIN IN THE REGION OF THE CERRO PRIETO GEOTHERMAL FIELD

ABSTRACT

In an analysis of local seismograms of seismic activity in the Mexicali Valley in the vecinity of the Cerro Prieto geothermal field, we have found that the attenuation of coda waves that dominate the seismogram of local events for times 2.5 times greater than the time of S-waves is extremely sensitive to the local volumetric structure in which such waves are propagated. Particularly in the region of the Cerro Prieto geothermal field, the heterogeneous structure of the sedimentary cover is reflected in extremely high dispersion of the coda waves, whose origin is quite probably the dispersion of body waves (5 hz - 12 hz) in the heterogeneous structure of deep sediments; for lower frequencies, the coda waves are composed of surface sedimentary waves and random waves that propagate in the shallowest structure of the sediments. The great heterogeneity in the structure of the sediments may be directly observed by comparing the amplitude spectrums of the S waves and of the coda waves (2.5 Ts), which are similar and have comparable values. The functional dependence of Q on frequency, for the frequencies studied (+hz - 12 hz), indicates a Q quotient (=250), in contrast to similar observations in the longitudinal structure of the south sector of the Imperial Fault, in which Q was found to increase with frequency (100 at 1 hz - 270 at 11 hz).

INTRODUCTION

On June 9, 1980, at approximately 03:28:20 GMT (June 8, 1980, 20:28 local time) an earthquake of a local magnitude of 6.1 occurred (Reyes, 1980; Anderson, J. and Simmons, R. 1982). The location of the epicenter by instruments was estimated to be 10 km southeast of the town of Guadalupe Victoria, BCN, near the surface trace of the Cerro Prieto Fault and to the southeast of the Cerro Prieto geothermal plant. The preliminary location of the epicenter and the estimate of its focal depth were possible thanks to the availability of logs (seismograms) of the RESCEP system (a CFE/IIE-CICESE project) operated by CICESE. The arrival times at the RESCEP system and at the stations of the Southern California Border Network, CEDAR, operated by Caltech, made it possible to provide a preliminary estimate of the focal coordinates of the principal event, which, in turn, served as a basis for planning subsequent field work to study the distribution of aftershocks in detail, in addition to the attenuation and scattering in the amplitude spectrum of the aftershocks. A few hours after the Victoria Event occurred, portable CICESE DCA-300 and UCSD-IGPP DCA-302 digital recording units were installed to supplement the coverage of the RESCEP system.

The RESCEP digital telemetric network consists of six stations distributed in the region of the Cerro Prieto geothermal plant within a radius of 20 km. Ten hours after the main event, it was possible to connect the digital seismic signals directly to the VHF-Telephone links between the RESCEP network and CICESE in Ensenada, entering through the ALMC line into the PRIME-350 system for the processing of seismic signals of the RESNOR system (Duarte, C.; Hinojosa, A.; Inzunza, L.; 1981).

The digital data base stored on discs and magnetic tapes of the PRIME-350 system were used in this study in conjunction with the data base on the Mexicali event in 1979 recorded on the CICESE DCA-300 and the UCSD-IGPP DCA-302 portable digital equipment.

The digital data base (RESCEP) consists of digital seismograms recorded at a sampling velocity of 60m/sec, an accuracy of 12 bits and a five-pole anti-alias filter with a cutoff frequency of 15 hz, as well as data recorded with portable DCA-300 and DCA-302 digital equipment with a sampling velocity of 100 m/sec on three channels with words of 12 bits and a five-pole anti-alias filter with a cutoff frequency of 30 hz. The process for demodulating, decoding, storing on discs and magnetic tape, as well as CRT screen analysis and editing have been described previously in the scientific literature (Brune et al., 1980; Duarte et al., 1981; Reyes et al., 1982).

Locating aftershocks

Ten hours after the principal event, it was possible to record the sequence of aftershocks by direct interphase through the ALMC lines between the telephone lines

and the PRIME-350 computer of the RESNOR system, as described previously. During 24 hours, it was possible to detect 50 events simultaneously at the six stations of the RESCEP (Red Sísmica de Cerro Prieto) system. Unfortunately, at the time of this event, the Universal time and labeling control system on each channel of the system was not in operation. Thus, the time of each component of the logs during the sequence are expressed in the local time of the PRIME-350 system. Since the recording routines to sychronize detection on each channel were not yet in operation, the relative times of signals on each channel are not reliable. The relative times of the P and S phases for a particular signal, however, are completely reliable.

The files for a particular event recorded at each of the RESCEP stations are edited at the TECTRONIX video terminal with the MUPPET program (Duarte, E.. et al. 1981) , with which it is possible to access a particular event stored on a disc or magnetic tape and to activate X-Y cursors to position a particular channel (X axis) or to read the arrival time of the signal required (Y axis). In this manner the P and S phase times are stored in a file, which is subsequently used in the HYPO 81 program to estimate the focal coordinates (X, Y, Z) and origin time for each of the events.

In order to determine the epicentral and focal coordinates of the S-phase and P-phase using relative times (Tsp), the value of the velocity ratio Vp/Vs must be assumed. Prior aftershock sequence studies on the 1978 Victoria Swarm (Reyes, 1979; Albores, 1980) and a detailed study of the aftershocks of the Mexicali Event, which occurred 48 hours after the main event (Wong, V. and Frez, J., 1982) obtained reliable estimates of the Vp/Vs ratio as being equal to 1.80. This is the value we have used in the calculations discussed in the present study, which is described below.

If we assume that the ratio Vp/Vs, as a funcion of depth, does not vary significantly in the region of the study (Fig.1), it is easily demonstrated that Ts/Tp = Vp/Vs for a vertically inhomogeneous setting, where Tp is the P-phase run time and Ts is the S-phase run time, from which it may be deduced that:

$$Tp = (Tsp) / (Vp/Vs - 1)$$

That is, the Tsp times enable us to estimate the P-phase run time directly from the seismogram, dependently from the estimated spatial coordinates of the hypocenter.

To calculate the P-wave run times in the local crust, we have used a stratified model of Vp compressional wave velocities refined through trail and error in a study by Wong, V. and Frez, J. (1982), in addition to the assumption that Tsp observations have a normal distribution, with scattering or variance = 0.2 sec and a mean = 0.

The results obtained from these calculations are listed in Table I and their spatial distribution is presented in Figure 1. In Table I, it may be seen that error bars in determining the epicenter and estimating the focal depth may only be estimated for a limited number of events. For residuals on the order of RMS = 0.25, with five stations, the errors in epicentral and focal depth estimates are about $\pm$ 4.5 km and $\pm$ 2.5 km respectively, and increase to $\pm$ 8.5 km and $\pm$ 16.5 km for events with a greater acceptable RMS = 0.52 sec. Most of the locations determined lie within the network (RESCEP) which allows for good azimuthal and depth control in the calculations. Nonetheless, we believe that the absolute hypocentral positions might change notably ($\pm$3 km) if a greater number of logs from a denser network of stations had been available for the study. We do not, however, believe that significant changes would occur in the relative positions.

As shown in figure 1, the distribution of aftershocks 10 hours after the main event is distributed along the northernmost part of the Cerro Prieto Fault and there are no aftershocks in the vecinity of the epicenter of the main event.

Figure 2 shows a profile of the aftershock depths along a northwest-southeast line parallel to the known trace of the Cerro Prieto Fault in which we can see that the aftershocks are distributed over a volume at an average depth of 10 km to the northwest. The cross section (NE-SW) shows the concentration of the aftershocks in a nearly circular region at a depth of 10 km and with a radius of $\pm$ 6 km, and their distribution does not suggest a dominant plain. Both cross-section profiles suggest a volumetric distribution within a circular ellipsoidal envelope whose main axis is aligned predominantly in the direction of the azimuth of the course of the Cerro Prieto Fault.

The distribution of aftershocks of the Victoria Event is complementary to the distribution of the epicenters of the March 1979 Victoria Swarm (Reyes, 1979), which are distributed along the four well-

defined trends (Reyes, A., 1978; Albores, A., 1980) reproduced in figure 1 for comparison. The distribution of depths taken along the profiles indicated in figure 1 are shown in figures 2 and 3. The surface projection of both sequences of seismic events shows that both distributions are complementary at a common volume.

Spectrum of the Aftershocks of the Victoria Event and the Mexicali Event.

The spectrum for each of the events listed in Table I was calculated for coda waves at different time runs recorded on the vertical (V) and horizontal (H) components. The spectrum was calculated using Fourier's fast transformation (FFT). Each estimate of the spectrum is weighed in accordance with Hamming's criterion for removing the effect of the lateral lobes caused by the finite longitude of the signal being analyzed. Some typical spectrums are shown in figure 4 at a time of 2.5 ts (ts = S-wave run time) over a time series of 5 sec. of longitude (300 samples), in conjunction with the complete seismogram and the spectrum of the S-wave.

As may be observed, the coda wave spectrum over a longitude of 5 sec. at a coda wave travel time of 2.5 ts is not significantly different from the spectrum of the S-wave packet. In fact, both are similar and of approximately the same amplitude.

Some of the statistical properties of the coda wave spectrum over a time window of 5 sec. have been analyzed, calculating the normalized average spectrum of all the events recorded at one particular station during the 24 hours of recording reported on in this study. For this calculation, we normalized each coda spectrum for a run time of 2.5 ts at a frequency of 6 hz. Typical spectrums are shown in figure 5, where we can see that the variance of the spectrum thus obtained is great but within acceptable error limits for frequencies less than 4 hz; for higher frequencies the variance diminishes, which indicates that the coda spectrums for all the events recorded at one single station are similar for frequencies greater than 4 hz and significantly different for lower frequencies (with reliability of 75%) probably owing to the combined effects of the volumetric structure between the station and the source (for tc = 2.5 ts) and the spectrum of the source.

Estimates of Apparent Attenuation in the Coda Waves.

We analyzed the attenuation of the spectral amplitude of the coda waves as a function of time by calculating the logarithm of the ratio of the coda spectrum (over a time window of 5 sec.) for a fixed reference time (to) in relation to a moving window of the amplitude spectrum as indicated below.

The spectral amplitude of the coda wave at a time (t) measured in relation to the origin time in the model proposed by K. Aki and B. Chouet (1975) is calculated by:

$$Ac(w/t) = Sc(w)\ t^{-a}\ \exp(-2\pi ft/2Qc) \quad (1)$$

where Sc (w) represents the coda wave source factor, Qc (w) is the intrinsic attenuation of the setting in which coda waves are propagated, and the constant a indicates geometric scattering (a = 0.5 for surface waves, a = 1.0 for body waves).

As illustrated in the seismograms of figure 4, the gradual decline in the coda amplitude may be analyzed by comparing the amplitude spectrum for different times and measuring the related Qc(w) values directly:

$$Ln = \frac{Ac(w,to)}{Ac(w,t)} = aLn\left(\frac{t}{to}\right) + \frac{w}{2Qc}(t - to) \quad (2)$$

In figures 6a, 6b and 6c, the values of the amplitude spectrum ratio of the coda wave train over a 5-second window are shown. The natural logarithms (Ec. 2) of the coda spectrum ratio at a run time of 20 sec for all the events, which are weighed by a moving spectrum window beginning at a time two and a half times greater than the S-wave run time and ending at times in which the signal-noise ratio is acceptable, were calculated for a total of 18 events that were located with sufficient accuracy. The epicenters are shown in figure 1. Each event was recorded simultaneously at the majority of the RESCEP stations (NVL, QKP, VER, TLX). The spectral ratios of the vertical and horizontal components were combined in a linear regression of the parameters of the model (a, Q^{-1}, Ec.2). The individual inversion of each component gives similar model parameter values. Thus, to increase the density of data and improve the resolution of the model, we included both components. Altogether, for each frequency (from 1.2 hz to 12 hz) there are 162 points that cover a run time range from 12 to 38 sec, equivalent to a sweep over a volume of 20 km to 60 km of an equivalent typical ellipsoidal dimension, centered on the area covered by the stations.

For each particular frequency, there is a system of 162 equations similar to

equation 2. The linear regression was carried out with both parameters but with a parameter values limited to a range between 0.0 and 3.0 with increases of 0.5. Due to the strong correlation between the elements of the matrix of coefficients (0.75 - 0.9), the simultaneous regression of both parameters of the model is unstable because of the quasi-singularity of the system. The linear regression of the Q^{-1} factor for each frequency is shown in figure 7, where the functional dependency of Q^{-1} on frequency has a bell-shape in which the curve increases as the a value increases (0.0, 0.5, 1.0) with a corresponding decrease in (Q^{-1}). For example, at a frequency of 6.6 hz, Q values increase progressively to: 180, 211 and 260. For the minimum and maximum frequencies (1.2 hz and 12 hz) corresponding values of (273, 980) and (255, 296, 353) respectively are obtained. Thus, depending on the coda-wave generation model, the attenuation of the amplitude spectrum is the result of a balance between geometric attenuation and the intrinsic attenuation of the setting in which the coda waves are propagated.

Similar studies of the aftershocks of the Mexicali Event (October 15, 1979, M=6.6, Fig. 1.a) are shown in figure 8. The behavior of the functional dependence of Q on the frequency is radically different for parameter values of geometric dispersion a = 0.0, 0.5. However, with a = 1.0 (Mexicali Event) and a = 0.0 (Victoria Event) in both sequences, values for the instrinsic attenuation Q of (257, 272, 338) and (69, 185, 260) respectively are obtained for frequencies near 1 hz, 6 hz and 12 hz.

Within the interval of frequencies from 5 hz to 12 hz, the behavior of both sets of Q estimates is similar and within the range of error of the estimates.

Discussion of the Results

In figure 7, it may be seen that, if if is assumed that the coda waves are caused by the interference body waves or sedimentary surface waves (a = 1.0, a = 0.5) scattered in the heterogeneous materials of the setting, the Q values in the interval of frequencies from 5 hz to 12 hz are constant and consistent with the S-wave values reported by other authors (Singh, et al., 1981). The values in figure 7 for lower frequencies, however, are extremely high and would indicate that they are caused by scattering in the deep structure of the crust.

In figure 8, it may be observed that, regardless of the origin of the coda waves (random waves, a = 0.0; surface waves, a = 0.5; body waves, a = 1.0), the Q models predict values expected for the region.

A reasonable model of the coda wave attenuation structure (Fig. 7) could be obtained by assuming Q = quotient, which would indicate (1) a gradual change in the composition of the coda waves from high frequency body waves to random waves at lower frequencies; (2) a gradual change from surface sedimentary waves to random waves; and in an extreme case (3) random waves. Comparing these results with similar studies of the aftershocks of the Mexicali earthquake, it may be observed that a law of Q = quotient in the frequency band analyzed would indicate that the generation mechanism is essentially through scattered body waves in the highly heterogeneous structure of the longitudinal structure of the Imperial Fault zone.

If we accept that the functional dependence of Q is constant in the interval of frequencies analyzed in this study and thus obtain consistent results of Q for both sequences of aftershocks (Mexicali and Victoria), the mechanism for generating coda waves in both cases would be of a different origin and extremely susceptible to the structure in which they are propagated. In contrast, the results of the aftershocks of the Mexicali earthquake with a = 0.0 and 0.5 give estimates of the Q value whose functional dependence on frequency is similar to the results of S-wave estimates in the same region (Singh, et al.). However, the values are considerably less than for coda waves (a = 0.0) and correspond to the lower level of estimates, in which case, the coda wave generation mechanism cannot be explained by the interference of S-body waves scattered in the heterogeneous material of the setting.

Acknowledgments

During the different stages of this study, valuable comments, criticism and suggestions were provided by Dr. Keiiti Aki of the Massachussets Institute of Technology, to whom we are deeply grateful for his continous interest and enthusiasm in the developments of this study.

The digital network of Cerro Prieto (RESCEP) was financed jointly by the Comisión Federal de Electricidad, through the Instituto de Investigaciones Eléctricas (IIE), and CICESE. The

enthusiastic participation of Mr. Fernández de la Garza, Dr. Pablo Mulás del Pozo and Mr. Sergio Mercado del IIE made the financing of the RESCEP system possible.

Mr. Mauro Medina and Dr. Jorge Valerdi of CICESE developed the RESCEP system; Mr. Carlos Duarte, Mr. Alejandro Hinojosa and Mr. Luis Inzunza developed the data collecting, storing and automatic processing systems with the PRIME-350 system. Their experience, technological capacity and enthusiasm in developing the entire system made the RESCEP system possible.

The enthusiastic participation of Rosa María Alvarez Tinajero in processing the data base and the skill of Dalilah Lara in editing the present manuscript also warrant full recognition.

The study was financed with resources of CICESE granted by the Secretary of Programming and Budget.

FIGURES

Fig.1a. Region of the study. Aftershocks of the Victoria event and swarm.

Fig.1b. Region of the study. Aftershocks of the Mexicali event (1979).

Fig.2. SE-NW profile.

Fig.3. SW-NE profile.

Fig.4a. Spectrums using the vertical component of QKP of the event 443-5.80 (Table 1a).

Fig.4b. Spectrums using the horizontal component of QKP of the event 443-5.80 (Table 1b).

Fig.4c. Spectrums using the vertical component of NVL of the event 443-5.80 (Table 1a).

Fig.4d. Spectrums using the NVL horizontal component of the 443-5.80 event (Table 1a).

Fig.5a. Spectral variation.

Fig.5b. Spectral variation.

Fig.5c. Spectral variation.

Fig.5d. Spectral variation.

Fig.6a. Spectral ratios for f=1.2 for different values of A.

Fig.6b. Spectral ratios for f=7.2 for different values of A.

Fig.6c. Spectral ratios for f=12.0 for different values of A.

Fig.7. Q^{-1} (f) of aftershocks of the Victoria event.

Fig.8. Q^{-1} (f) of aftershocks of the Mexicali event.

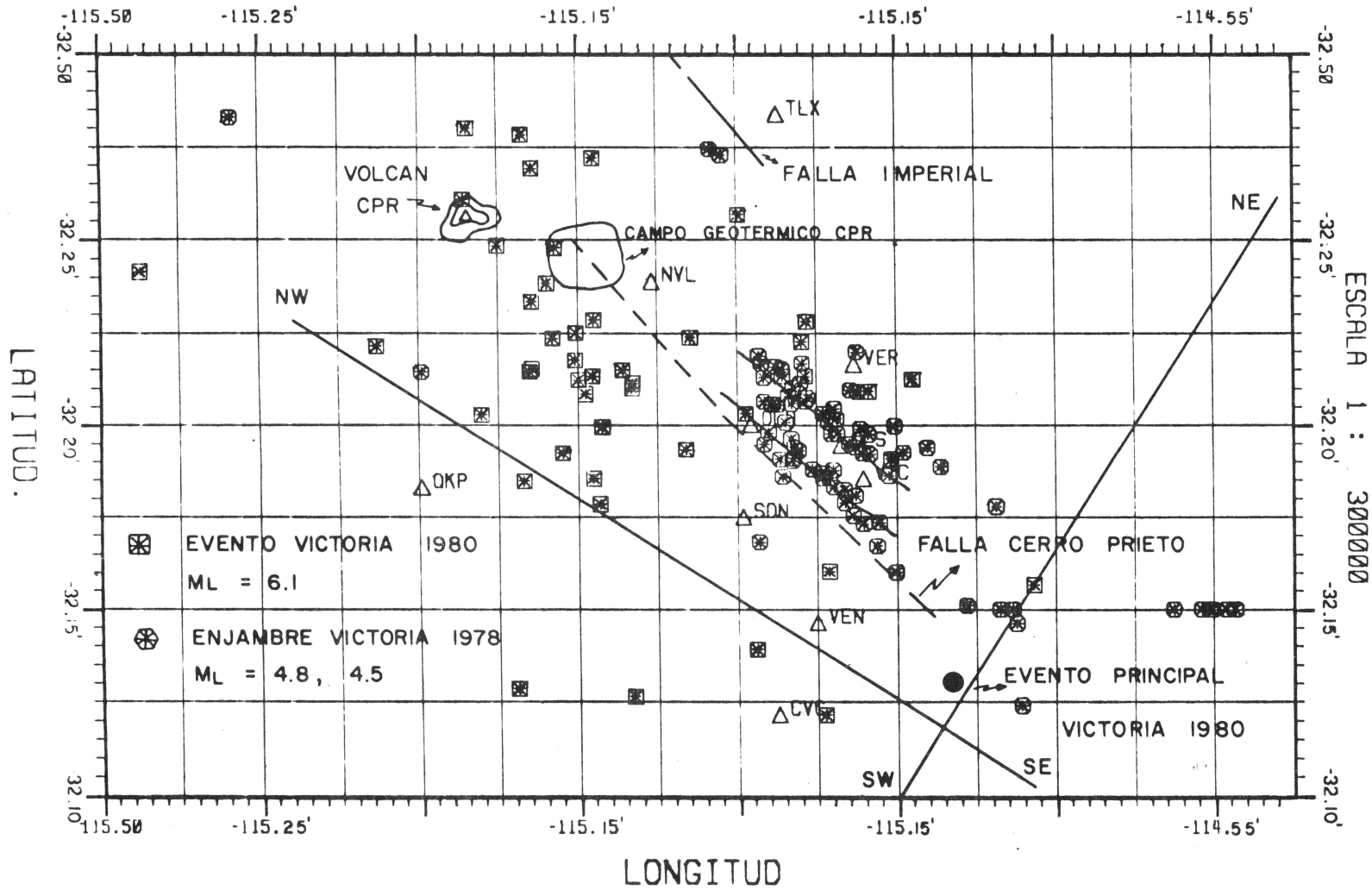

Fig. 1a Región de estudio. Replicas del evento y enjambre Victoria

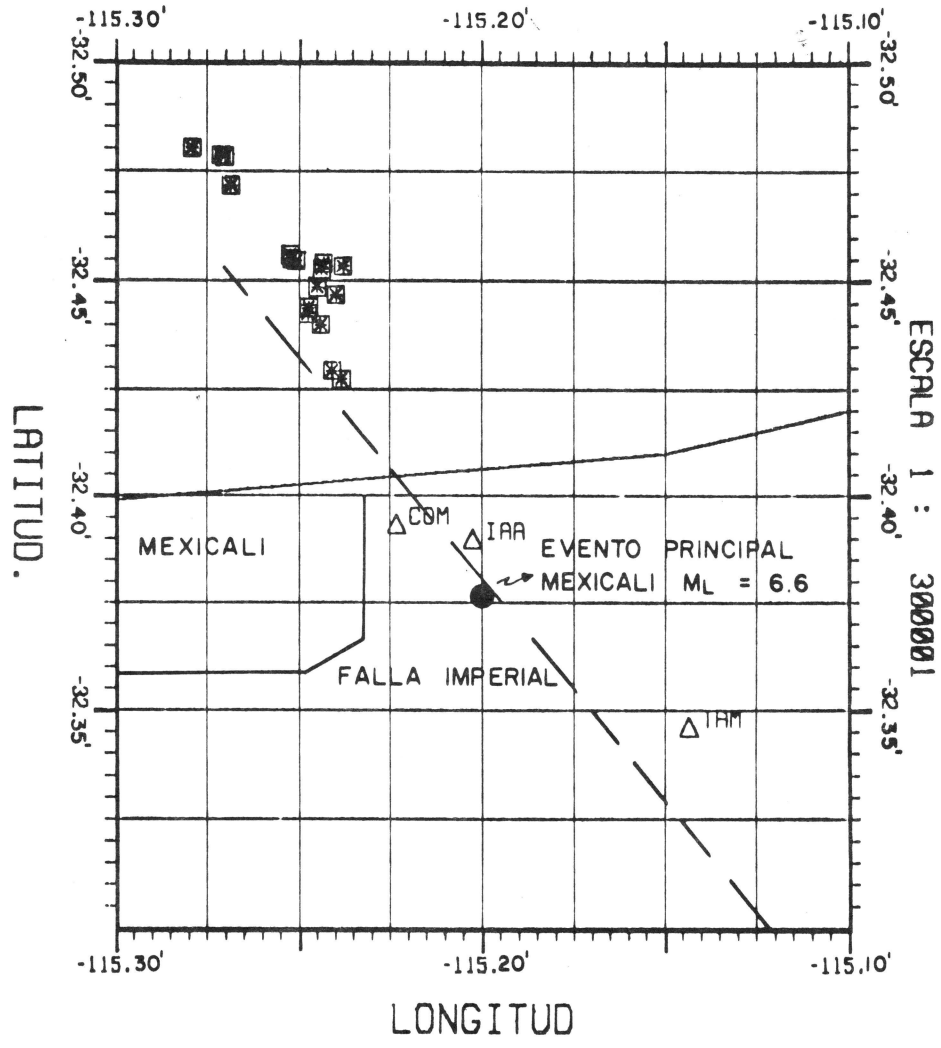

Fig. I b Región de estudio. Replicas del evento Mexicali (1979)

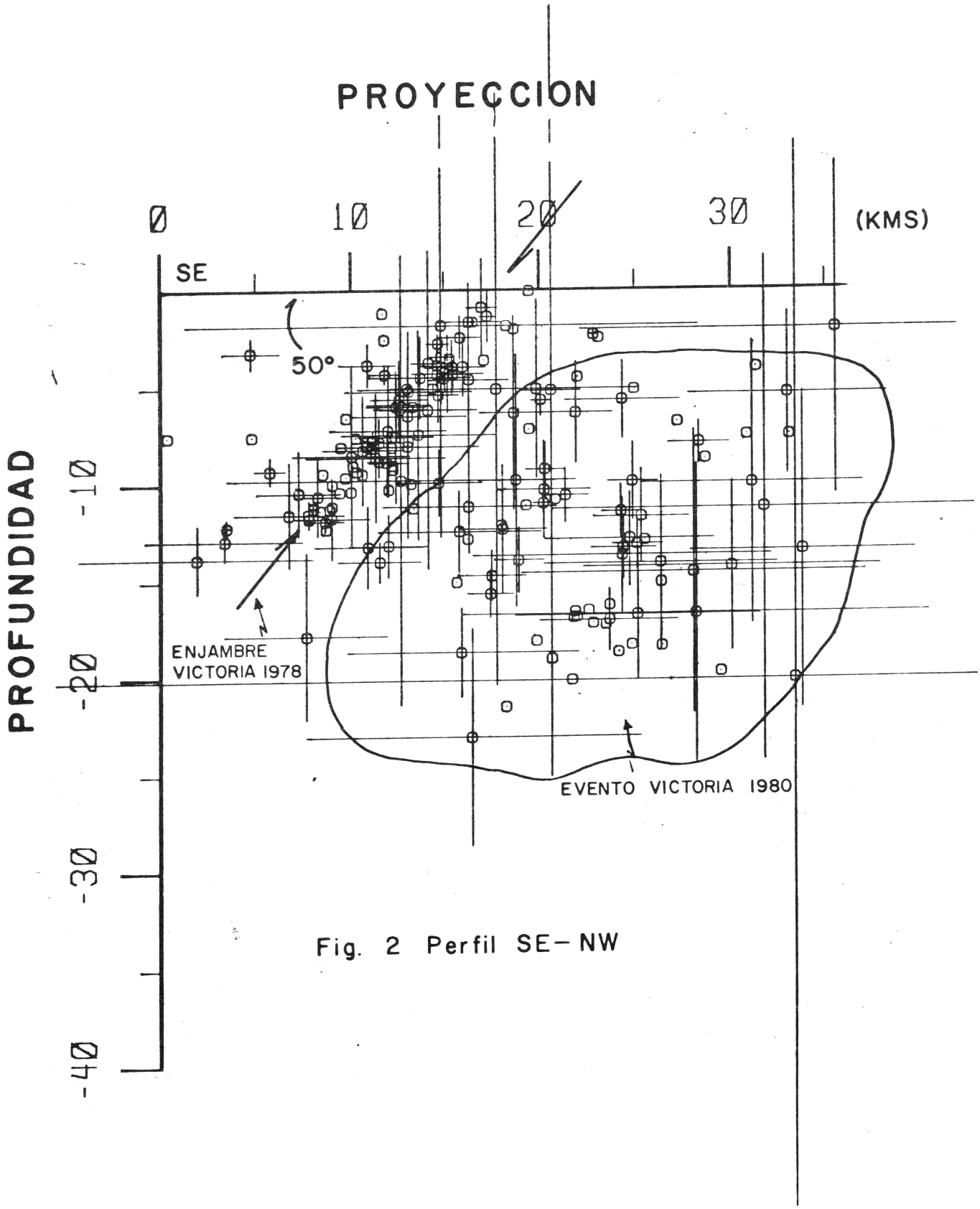

Fig. 2 Perfil SE–NW

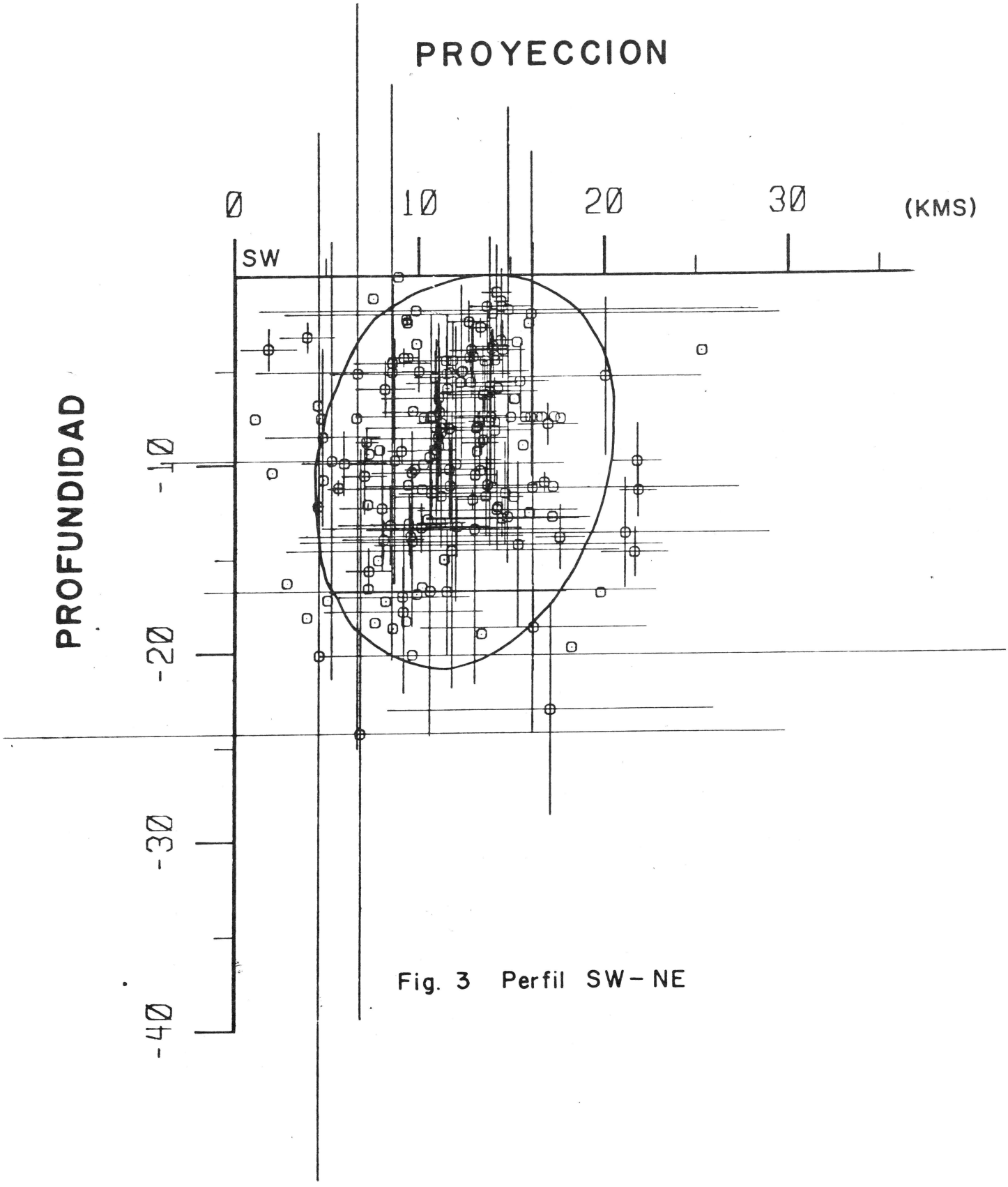

Fig. 3 Perfil SW – NE

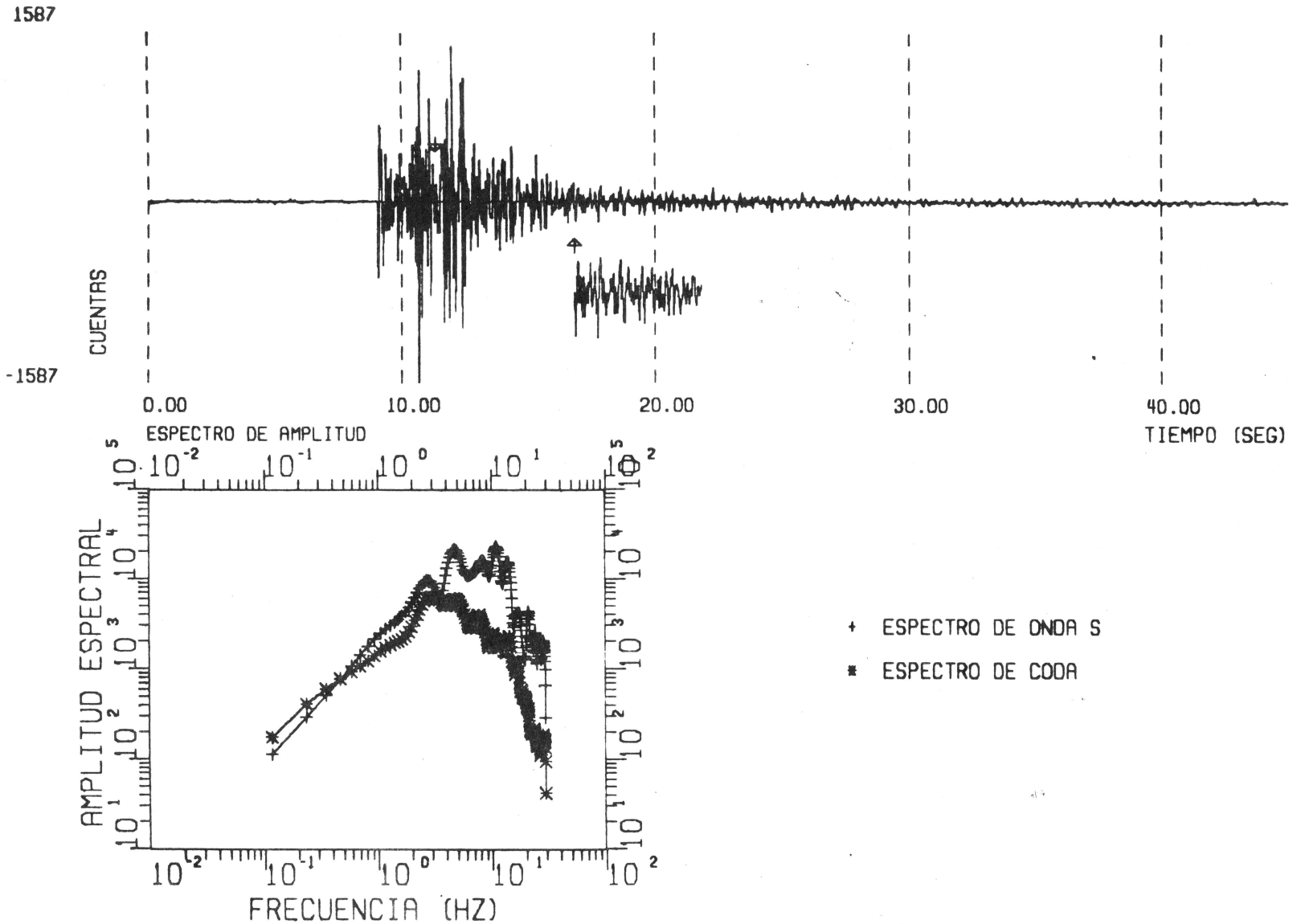

Fig. 4a Espectros utilizando componente vertical de QKP del evento 443-5.80 (tabla Ia)

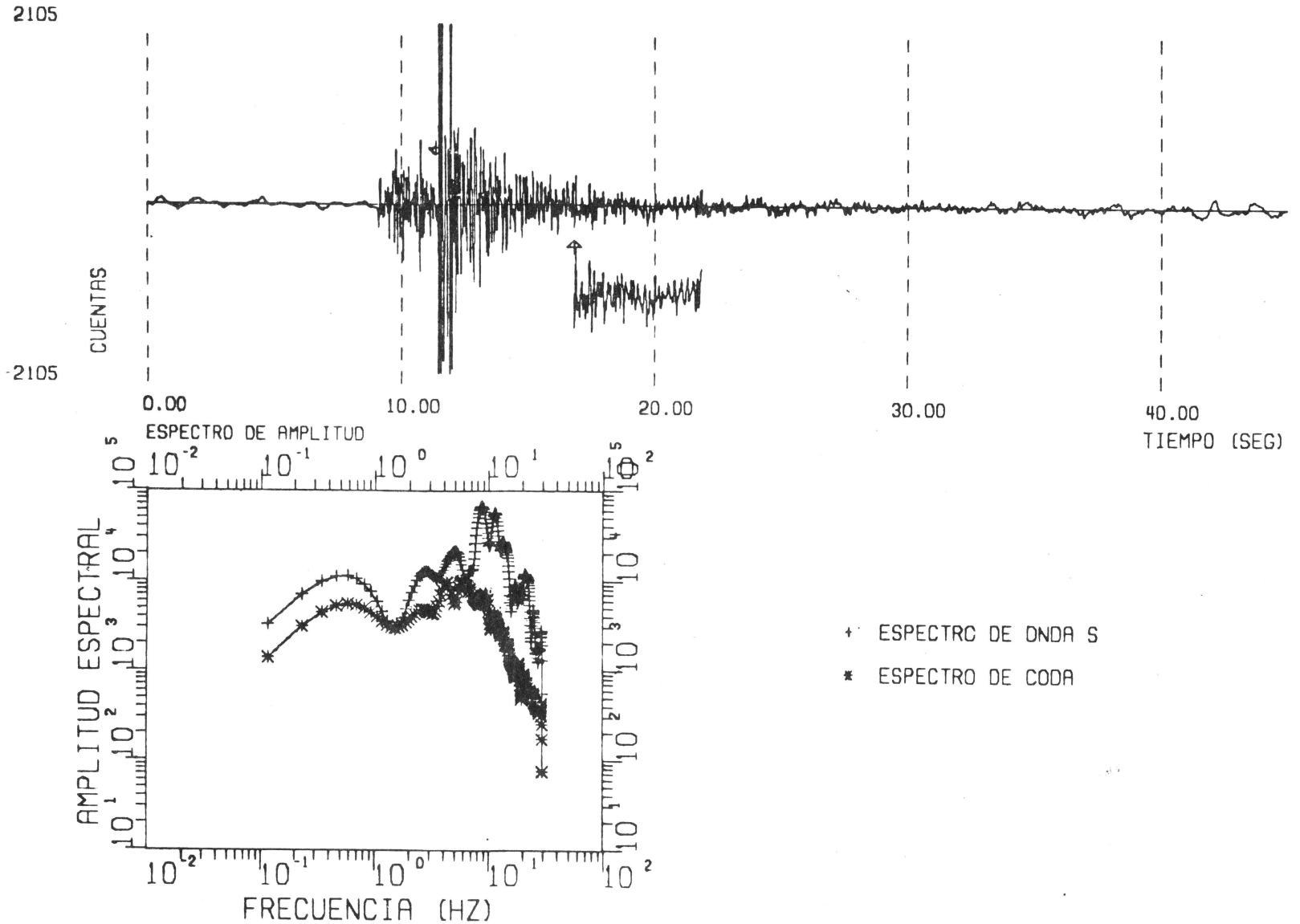

Fig. 4 b Espectros utilizando componente horizontal de QKP del evento 443– 5.80 (tabla 1 b)

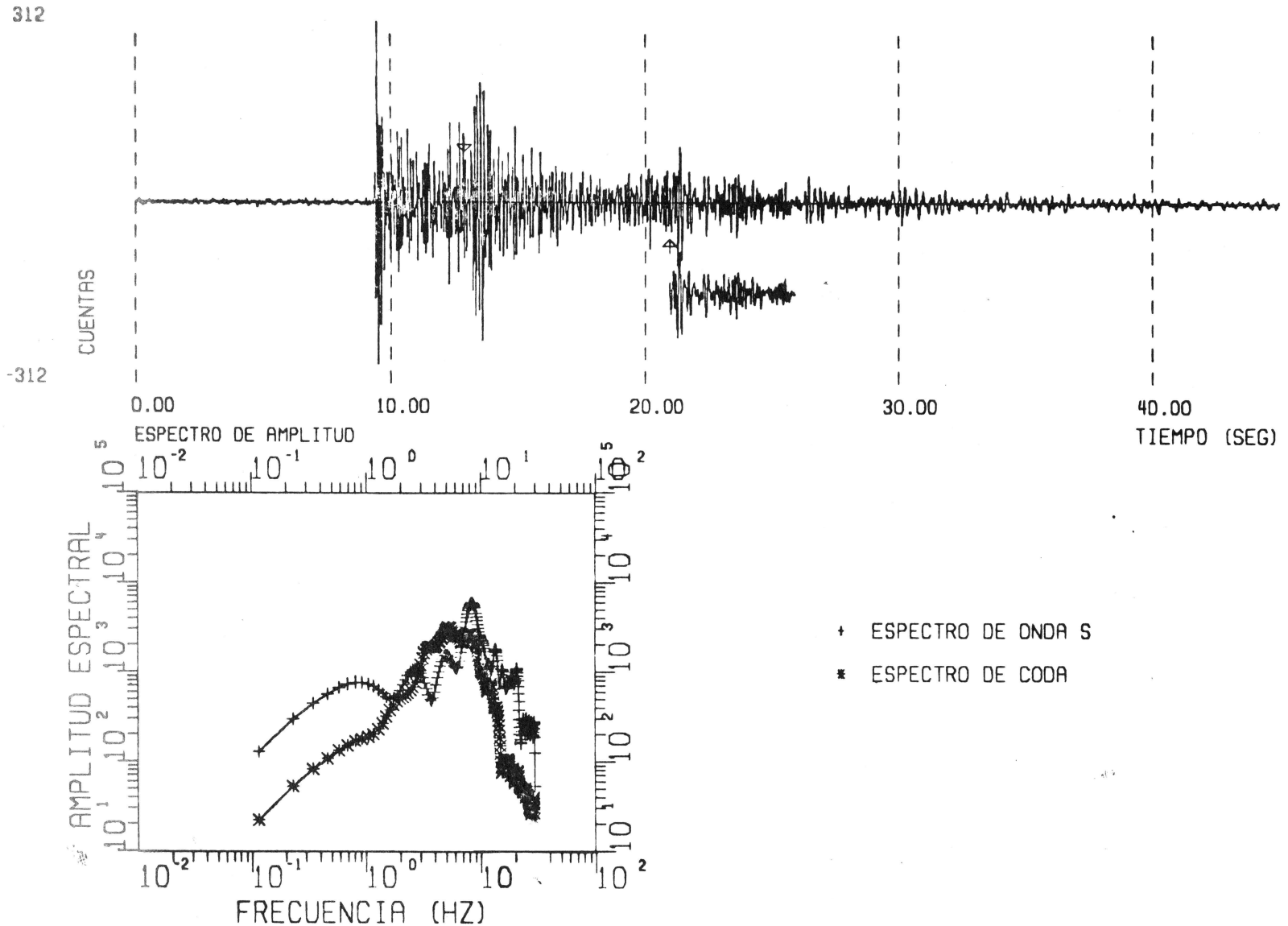

Fig. 4c Espectros utilizando componente vertical de NVL del evento 443 – 5.80 (tabla-1a)

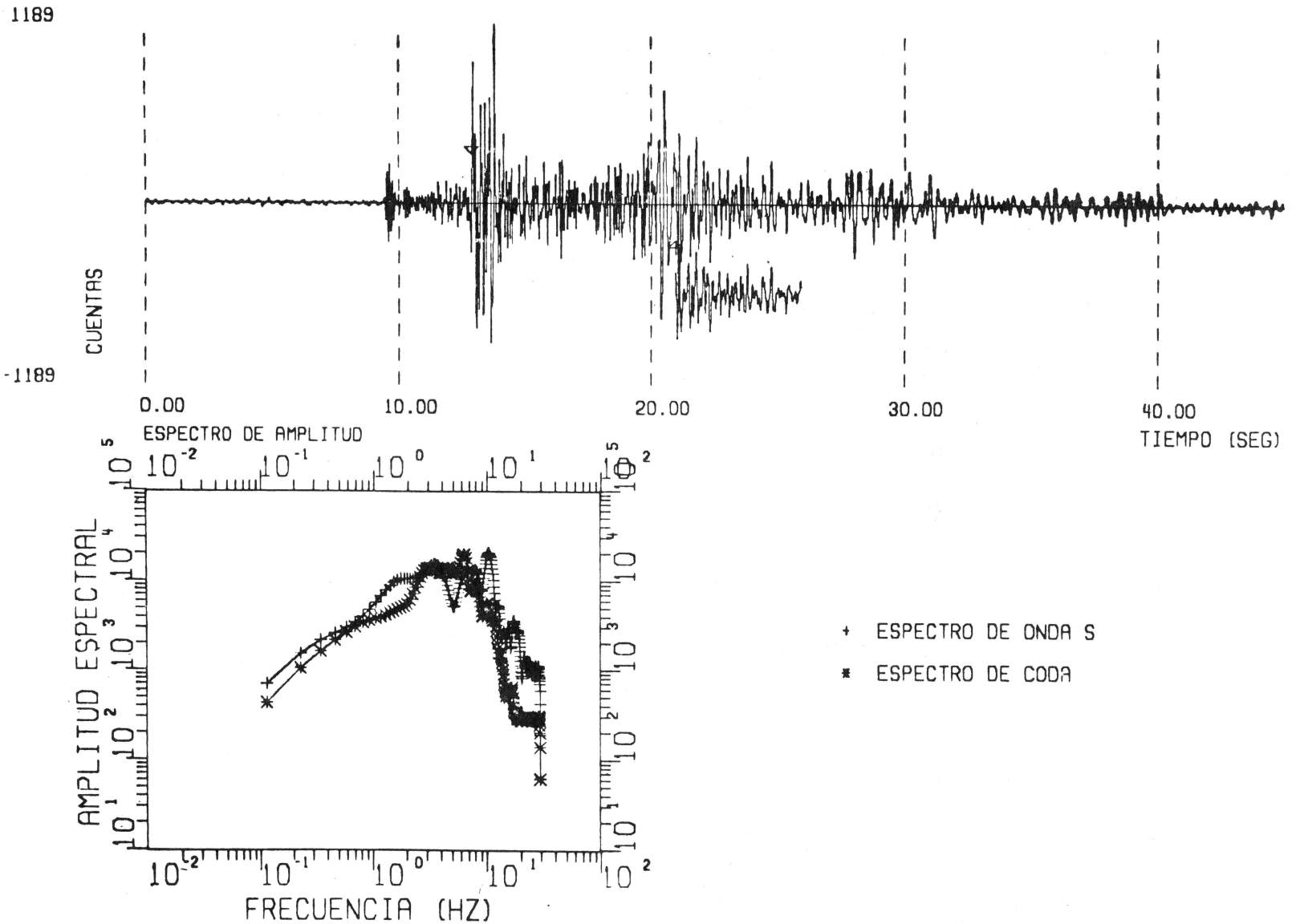

Fig. 4d. Espectros utilizando componente horizontal NVL del evento 443 - 5.80 (tabla 1a)

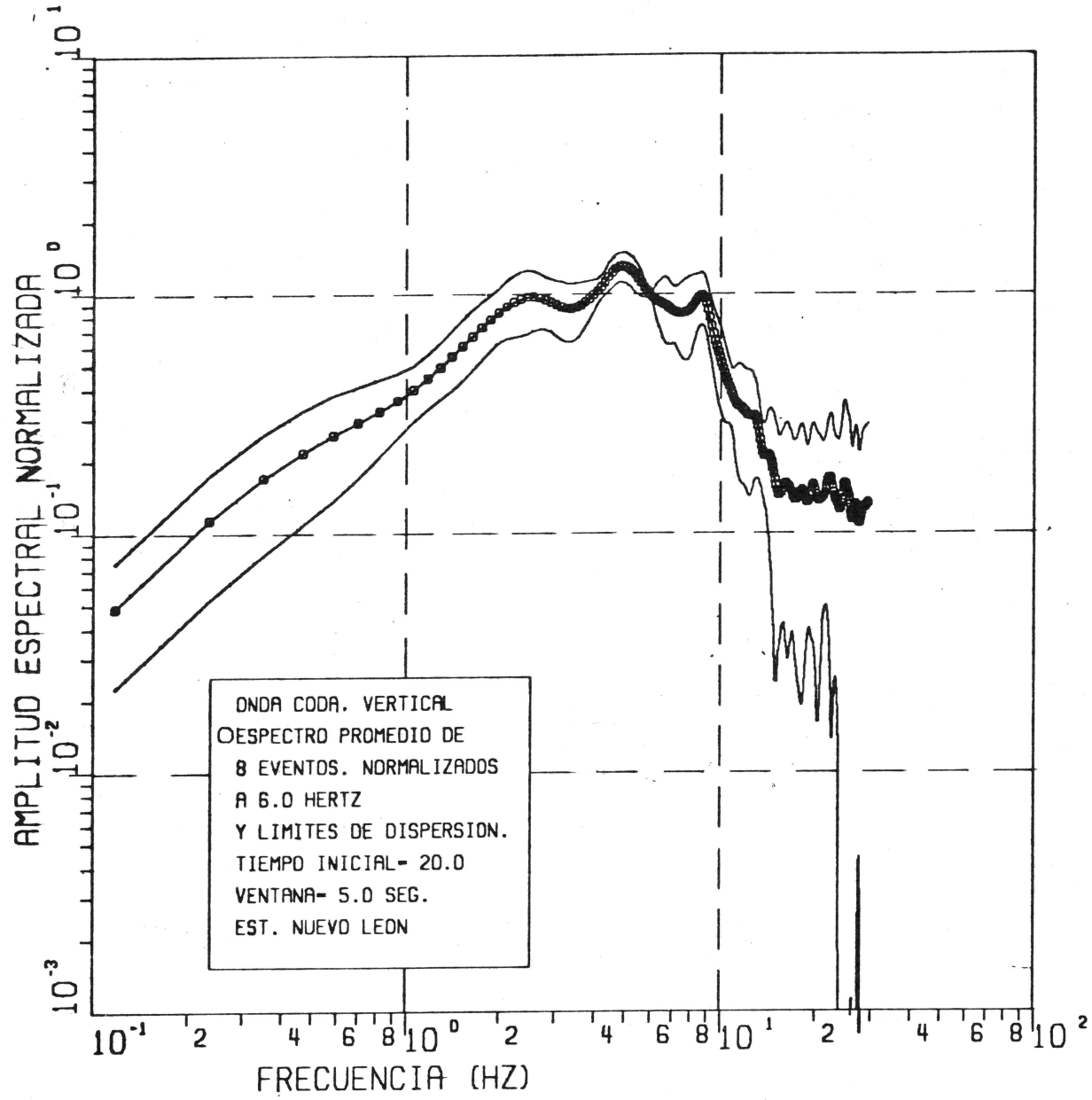

Fig. 5a Variación Espectral

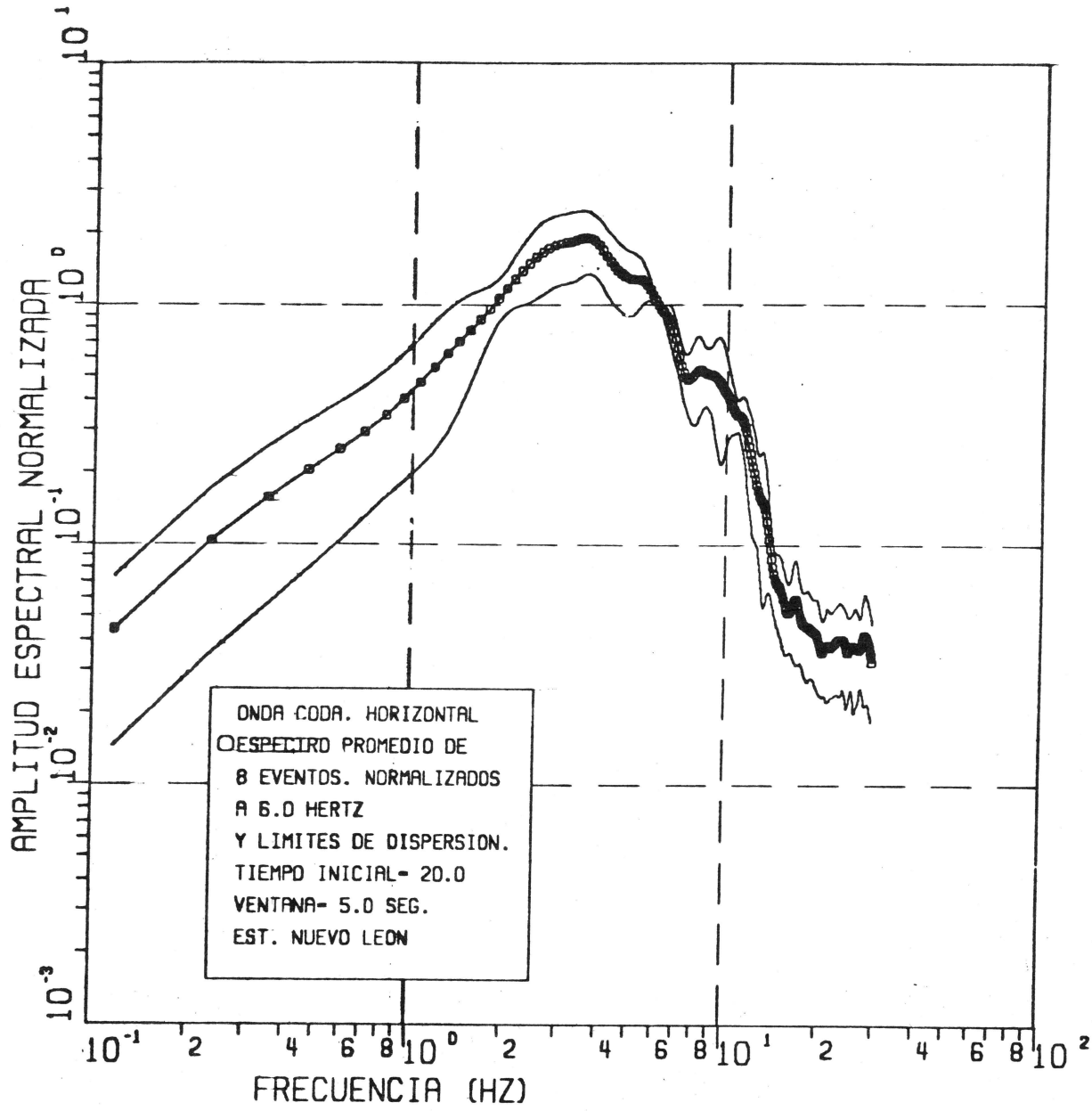

Fig. 5b Variación Espectral

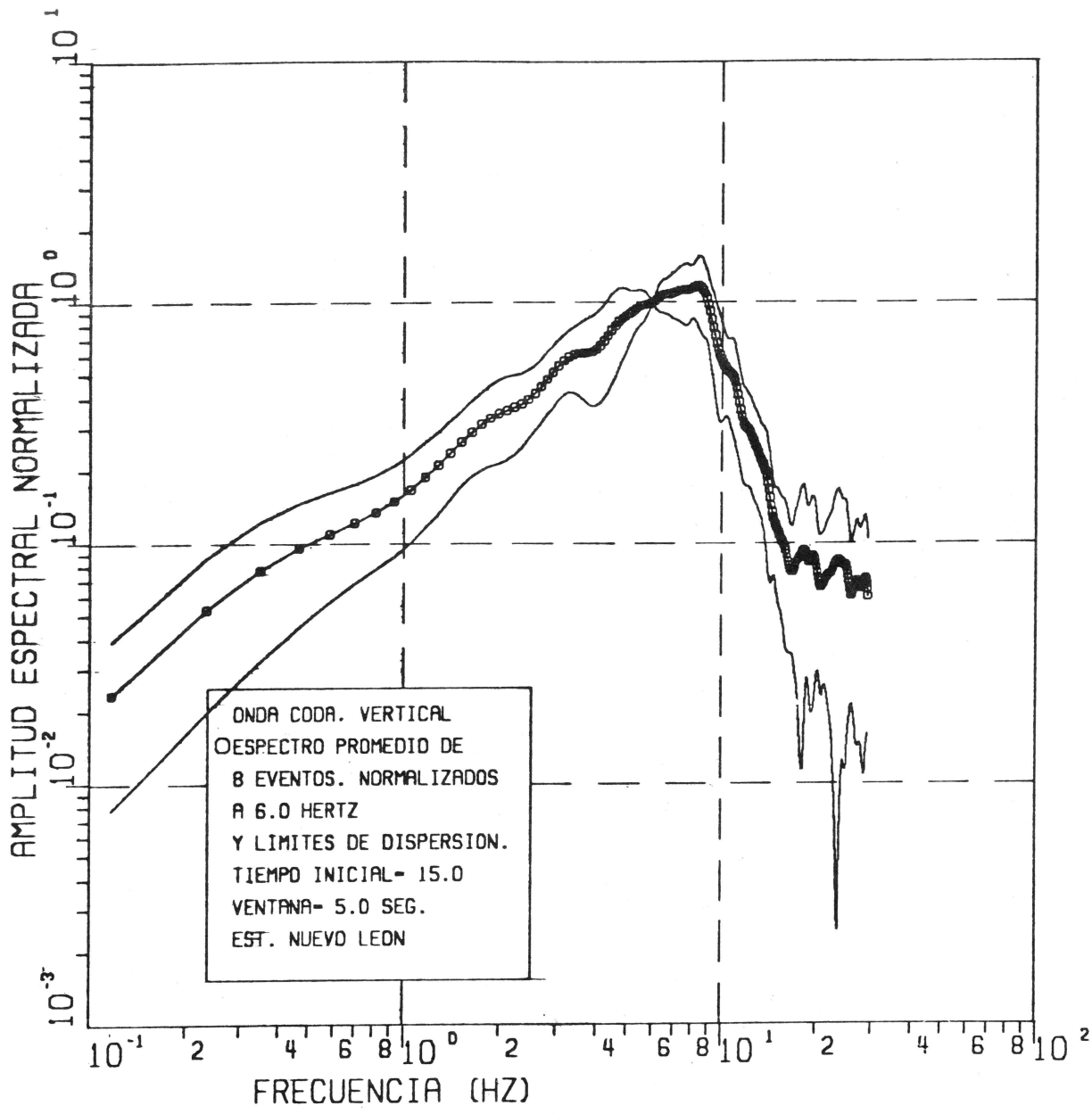

Fig. 5c Variación Espectral

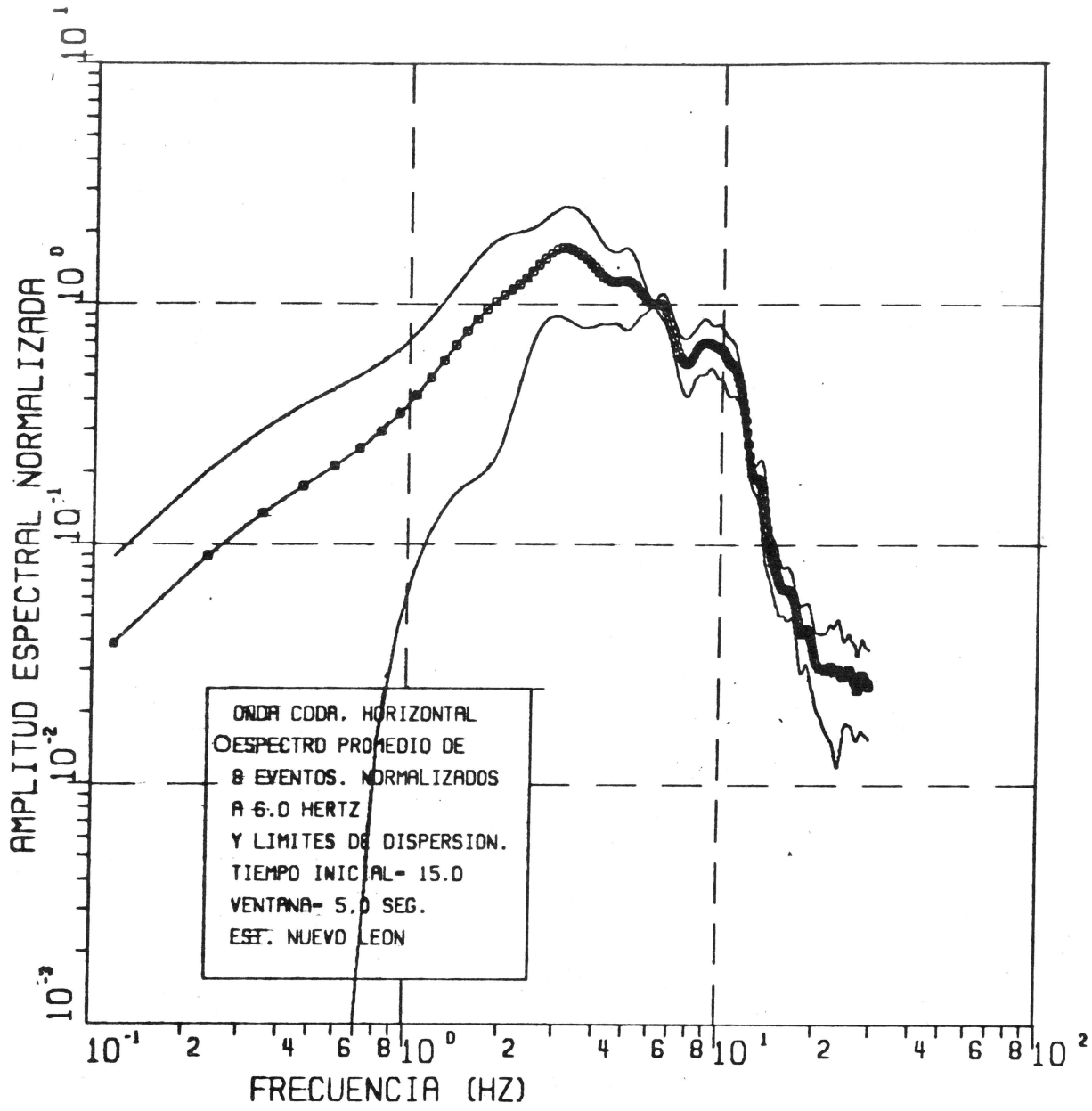

Fig. 5 d Variación Espectral

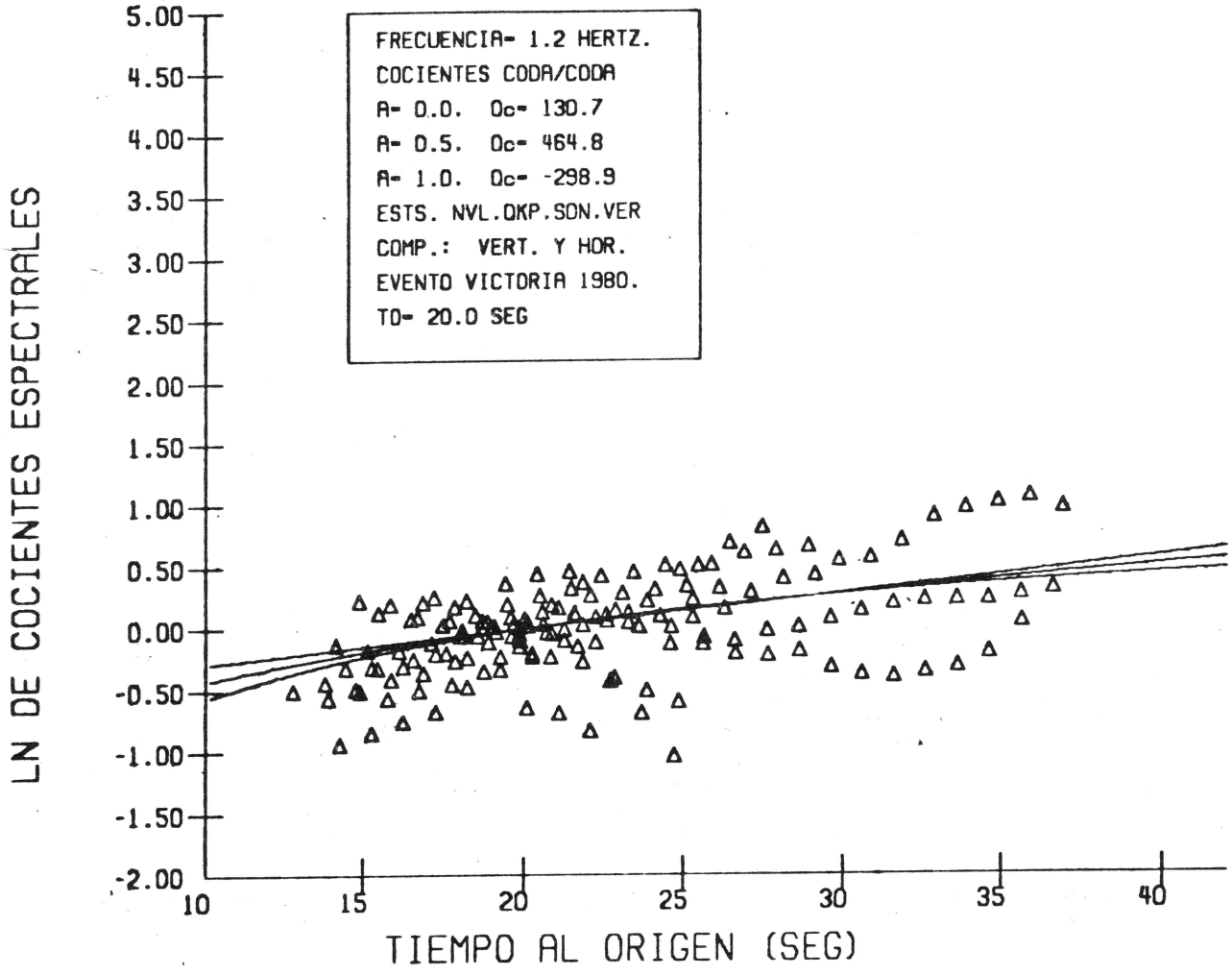

Fig. 6 a Razones Espectrales para f= 1.2 para diferentes valores de A.

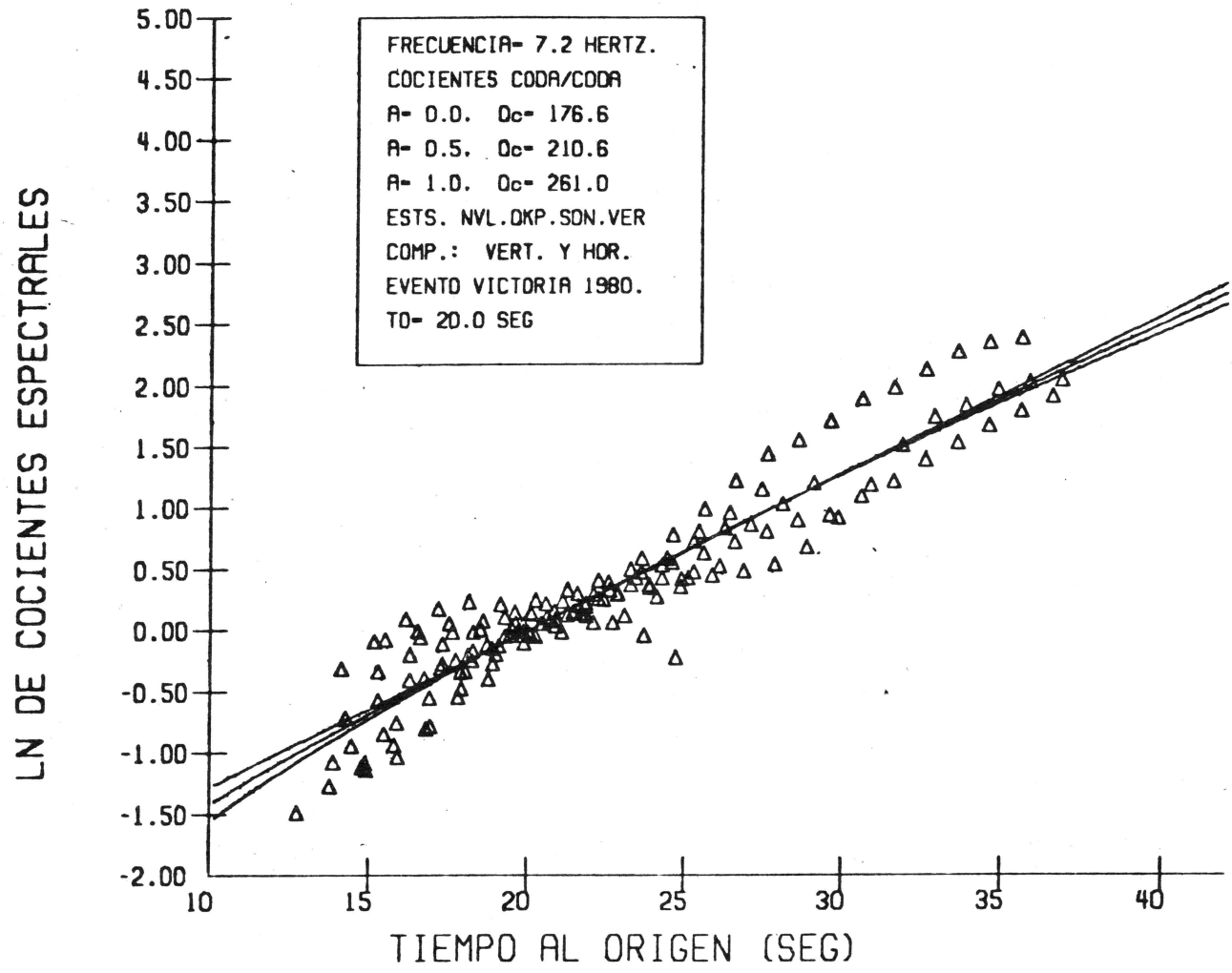

Fig. 6 b Razones Espectrales para f=7.2 para diferentes valores de A.

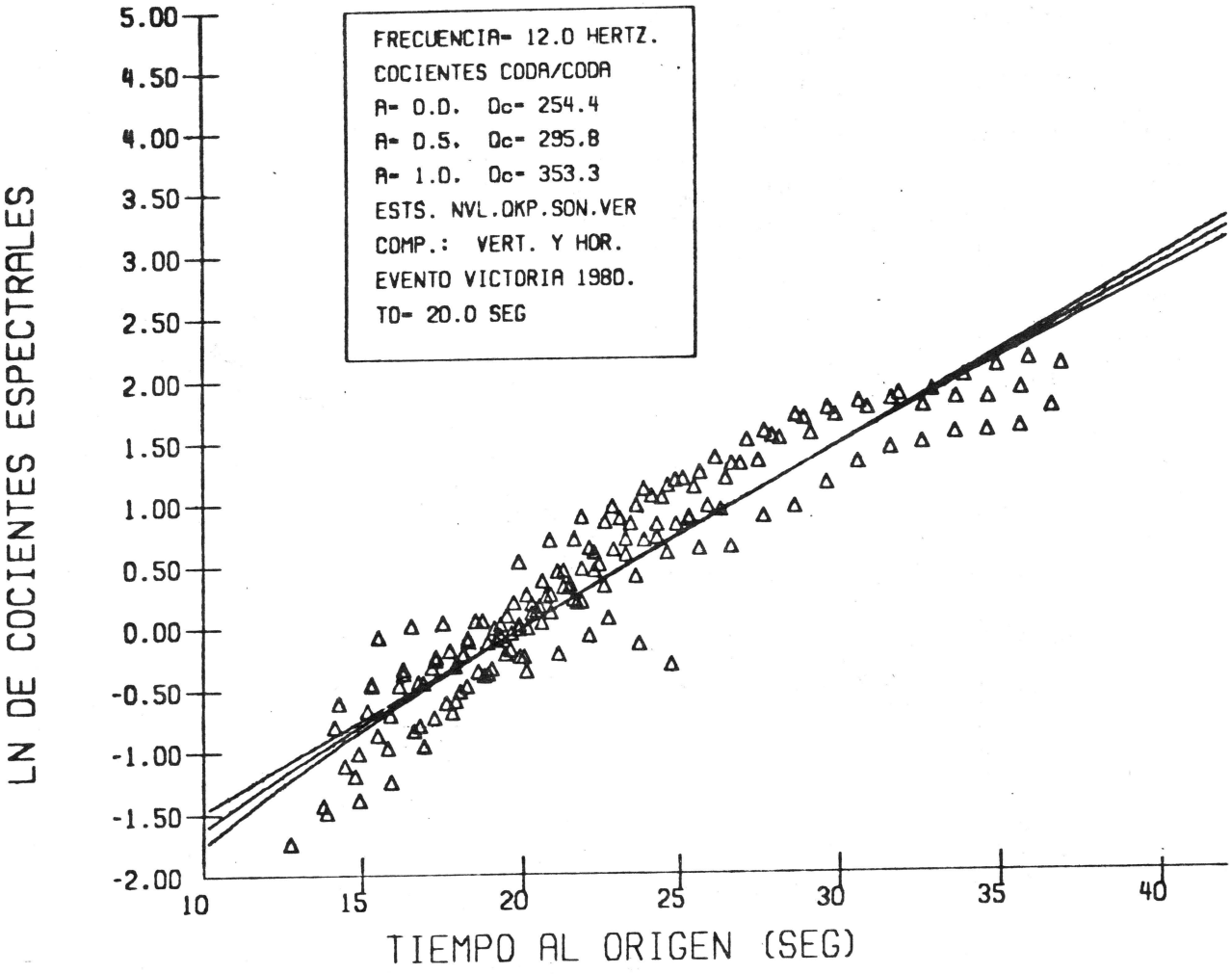

Fig. 6c Razones Espectrales para f = 12.0 para diferentes valores de A

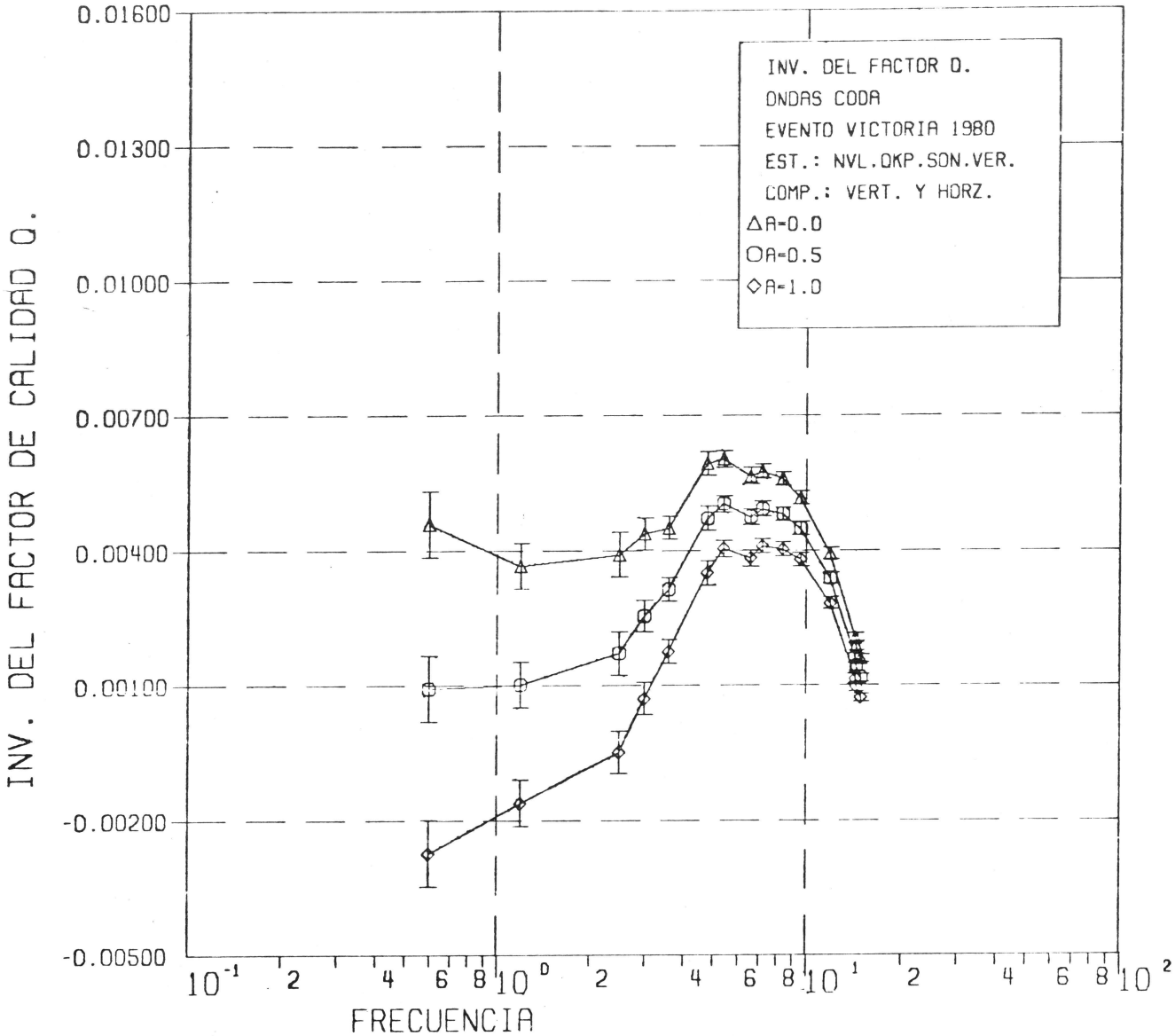

Fig. 7 Q^{-1} (f) de réplicas del evento Victoria.

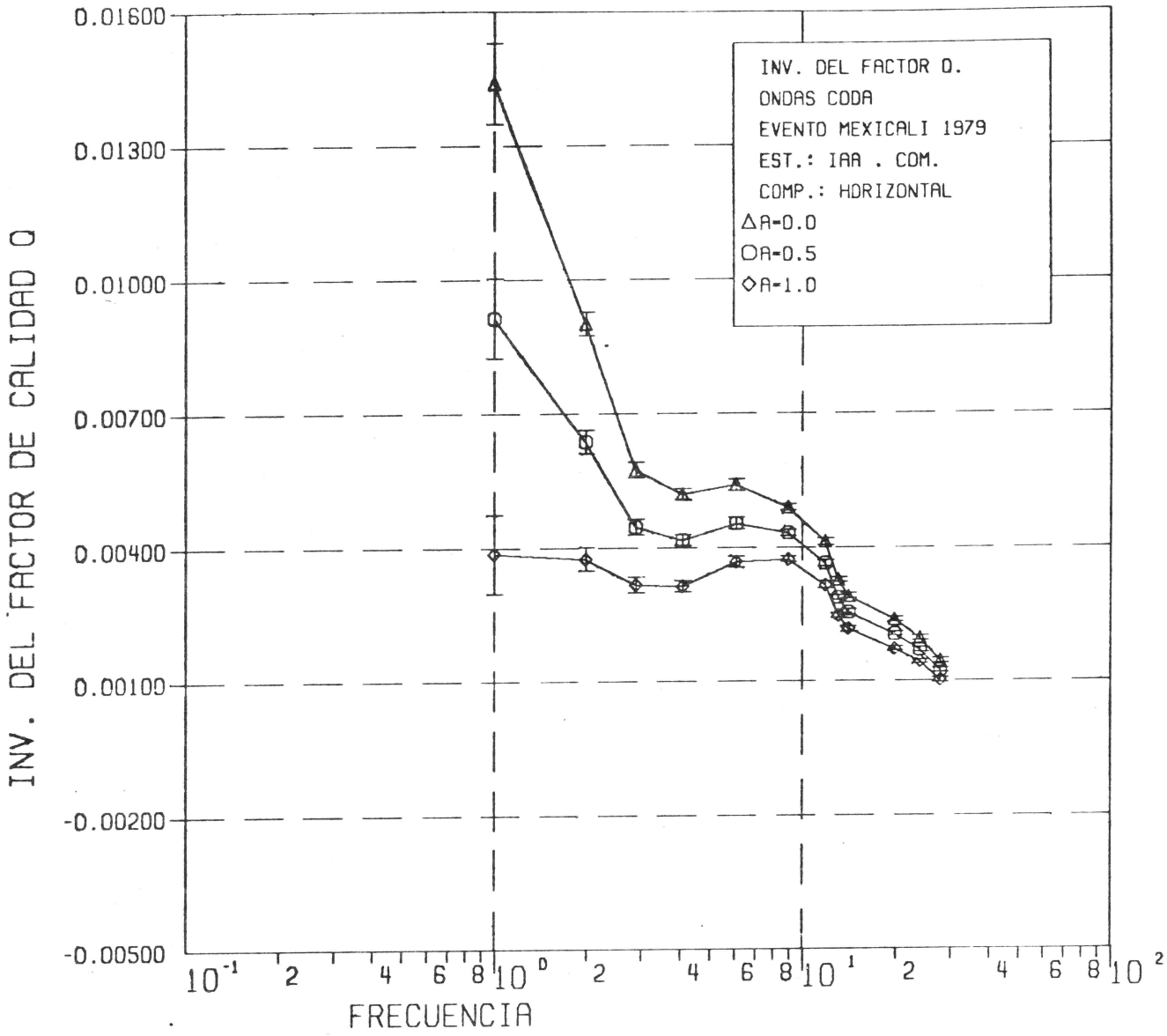

Fig. 8 $Q^{-1}(f)$ de réplicas del evento Mexicali.

EVENTO VICTORIA

DATE	ORIGIN	LAT N	LONG W	DEPTH	MAG	NO	GAP	DMIN	RMS	ERH	ERZ	QM
800610	336 6.64	32-21.23	115-14.98	18.69		4	161	6.1	0.03			C1*
800610	341 14.32	32-21.77	115-15.09	18.30		4	174	5.5	0.10			C1*
800610	342 1.34	32-21.14	115-13.28	16.87		4	127	5.2	0.06			C1*
800610	354 3.58	32-21.50	115-13.59	16.52		4	139	4.7	0.24			C1*
800610	421 3.07	32-19.24	115-15.49	17.17		3	146	7.2	0.01			C1*
800610	432 59.50	32-18.48	115-16.72	16.26		4	167	5.0	0.07			C1
800610	438 3.08	32-17.85	115-14.32	18.09		4	180	7.1	0.09			C1*
800610	443 5.80	32-12.64	115-13.28	9.95		4	282	10.5	0.03			C1*
800610	5 9 59.07	32-22.50	115-15.05	12.91		3	232	10.9	0.07			C1
800610	533 57.96	32-21.00	115-13.31	20.12		4	126	5.5	0.07			C1
800610	538 9.48	32-20.93	115- 5.87	2.52		4	252	1.51	1.62			D1
800610	615 58.81	32-22.26	115- 7.96	18.67		5	119	2.8	0.16	6.1	2.3	D1
800610	632 4.53	32-28.00	115-18.46	2.00		5	260	11.8	0.51	13.4	8.6	D1
800610	633 5.75	32-20.85	115-14.76	17.24		3	262	6.5	0.02			C1
800610	638 2.65	32-30.95	115-13.04	4.00		3	331	13.0	0.25			C1
800610	645 0.37	32-12.85	115-16.93	21.47		3	283	11.1	0.01			C1
800610	650 2.19	32-22.82	115- 7.81	12.80		4	207	3.2	0.44			D1
800610	7 2 3.03	32-27.20	115-14.49	19.76		4	281	6.7	0.01			C1
800609	8 2 2.95	32-21.33	115- 8.58	12.42		5	115	3.6	0.17	4.3	2.1	D1
800609	810 58.73	32-23.35	115-16.45	16.70		5	202	6.0	0.35	12.2	7.7	D1
800609	820 1.37	32-19.34	115-11.61	5.08		5	121	4.4	0.44	7.4	15.3	D1
800609	826 1.56	32-23.85	115-15.97	14.58		5	202	5.2	0.30	9.0	7.3	D1
800609	840 1.03	32-26.92	115-16.43	11.25		5	238	8.1	0.37	11.1	13.0	D1
800609	843 58.58	32-13.92	115- 9.42	10.39		3	277	6.7	0.03			C1
800609	9 3 0.11	32-21.53	115-16.44	15.07		4	191	7.4	0.17			C1
800609	9 7 4.41	32-27.83	115-16.74	7.50		4	289	9.7	1.23			D1
800609	912 0.19	32-20.33	115- 9.74	11.14		5	116	5.2	0.19	4.6	2.4	D1
800609	913 6.10	32-18.55	115-14.53	10.78		4	162	7.6	0.01			C1
800609	915 7.87	32-12.15	115- 7.27	7.50		4	295	10.7	0.19			C1
800609	917 1.11	32-21.46	115-16.53	18.37		4	191	7.6	0.02			C1
800609	920 0.47	32-26.09	115-18.59	13.45		5	246	10.1	0.22	5.9	8.2	D1
800609	920 3.34	32-22.36	115-15.79	14.09		5	184	5.7	0.21	6.1	4.5	D1
800609	924 0.27	32-15.67	115- 0.69	5.66		4	318	14.2	0.72			D1
800609	945 7.91	32-22.86	115-14.50	16.76		5	176	3.5	0.19	6.4	3.3	D1
800609	951 1.16	32-25.68	115- 9.94	16.84		4	148	5.4	0.07			C1
800609	1012 4.78	32-24.85	115-17.53	9.97		5	227	7.8	0.21	5.8	7.3	D1
800609	1021 1.50	32-20.29	115-18.04	6.80		3	193	4.7	0.01			C1
800609	1045 59.90	32-21.33	115- 7.86	1.79		5	128	2.5	0.89	13.5	10.9	D1
800609	12 4 3.06	32-24.79	115-15.72	8.72		4	210	5.1	0.03			C1
800609	1948 9.50	32-22.14	115-21.30	20.13		5	257	7.4	0.88	38.8	27.8	D1
800609	1955 4.67	32-21.33	115-14.54	17.03		5	155	5.6	0.10	3.6	1.6	D1
800609	20 8 5.64	32-21.26	115- 4.48	7.58		3	284	13.7	0.02			C1
800609	2018 1.19	32-22.39	115-11.46	19.02		4	141	3.4	0.15			C1
800609	2026 2.26	32-19.96	115-14.24	16.59		4	175	7.7	0.23			C1
800609	2042 6.60	32-24.14	115-28.71	12.59		4	308	17.5	0.22			C1
800609	21 4 4.34	32-16.04	115- 7.13	9.43		3	288	16.9	0.13			C1

* EVENTOS EMPLEADOS PARA LA ESTIMACION DE Q DE ONDAS CODA
EVENTS USED FOR THE Q ESTIMATE OF CODA WAVES

TABLA 1-A

EVENTO MEXICALI

DATE	ORIGIN	LAT N	LONG W	DEPTH	MAG	NO	GAP	DMIN	RMS	ERH	ERZ	QM
791016	1916 52.10	32 45.51	115 25.21	8.71		17	84	11.6	0.06	0.3	0.3	B1*
791016	2027 54.07	32 44.39	115 24.73	8.91		14	88	13.7	0.07	0.4	0.4	B1*
791017	355 35.21	32 48.02	115 27.91	7.45		27	68	4.8	0.09	0.3	0.3	A1*
791017	934 59.00	32 45.35	115 23.79	9.17		12	77	4.4	0.09	0.5	0.3	A1
791017	937 59.39	32 45.47	115 25.09	9.15		22	76	5.3	0.07	0.3	0.2	A1*
791017	2219 44.27	32 45.27	115 24.38	8.92		23	77	4.5	0.07	0.2	0.2	A1*
791017	23 7 3.64	32 44.86	15 24.50	8.21		11	118	12.9	0.05	0.4	0.4	A1
791018	6 4 14.93	32 44.26	115 24.76	8.36		12	80	14.3	0.06	0.3	0.4	B1
791018	1152 47.01	32 44.00	115 24.41	8.89		22	81	13.7	0.09	0.3	0.4	B1*
791018	23 9 7.98	32 47.17	115 26.87	8.62		9	107	8.5	0.08	0.7	0.6	B1
791020	924 7.54	32 45.60	115 25.24	8.42		11	95	11.4	0.03	0.2	0.2	B1
791020	1443 29.86	32 47.85	115 27.13	8.61		12	87	7.3	0.09	0.5	0.4	A1
791021	1020 35.54	32 42.74	115 23.83	8.00		17	93	6.8	0.14	0.6	0.6	B1*
791020	1135 32.89	32 44.68	115 23.98	8.23		24	85	3.2	0.10	0.4	0.3	A1*
791021	19 4 12.52	32 45.41	115 24.32	9.14		21	130	3.6	0.10	0.5	0.3	B1*
791021	1954 35.75	32 42.93	115 24.09	7.67		21	93	7.2	0.16	0.6	0.6	B1*
791022	043 5.87	32 47.82	115 27.03	9.23		19	77	7.3	0.08	0.3	0.3	A1*

* EVENTOS EMPLEADOS PARA LA ESTIMACION DE Q DE ONDAS CODA
EVENTS USED FOR THE Q ESTIMATE OF CODA WAVES

TABLA I - b